Research Article | Vol. 29, No. 9 / 26 April 2021 / Optics Express 12958
Optics EXPRESS

Terahertz magnetoplasmon resonances in coupled cavities formed in a gated two-dimensional electron gas

S. J. Park,[1] S. Zonetti,[2] R. S. Parker-Jervis,[1] J. Wu,[3] C. D. Wood,[1] L. H. Li,[1] A. G. Davies,[1] E. H. Linfield,[1] O. Sydoruk,[2] and J. E. Cunningham[1,*]

[1]School of Electronic and Electrical Engineering, University of Leeds, Woodhouse Lane, Leeds, LS2 9JT, United Kingdom
[2]Department of Electrical and Electronic Engineering, Imperial College London, South Kensington Campus, London, SW7 2AZ, United Kingdom
[3]Research Institute of Superconductor Electronics, School of Electronic Science and Engineering, Nanjing University, Nanjing 210023, China
*j.e.cunningham@leeds.ac.uk

Abstract: We report on both experiments and theory of low-terahertz frequency range (up to 400 GHz) magnetoplasmons in a gated two-dimensional electron gas at low (<4K) temperatures. The evolution of magnetoplasmon resonances was observed as a function of magnetic field at frequencies up to ~400 GHz. Full-wave 3D simulations of the system predicted the spatial distribution of plasmon modes in the 2D channel, along with their frequency response, allowing us to distinguish those resonances caused by bulk and edge magnetoplasmons in the experiments. Our methodology is anticipated to be applicable to the low temperature (<4K) on-chip terahertz measurements of a wide range of other low-dimensional mesoscopic systems.

Published by The Optical Society under the terms of the Creative Commons Attribution 4.0 License. Further distribution of this work must maintain attribution to the author(s) and the published article's title, journal citation, and DOI.

1. Introduction

The terahertz (THz) frequency plasmonic response of mesoscopic systems (with length scales ranging from 100s of nanometers to a few microns) is of increasing interest for a wide range of potential device applications, including amplitude and phase modulators [1,2], emitters [3], amplifiers [4], and detectors [5]. To understand and optimize device characteristics fully, including the spatial distribution of plasmonic modes, various modalities of scanned near-field microscopy have recently been developed. For example, near-field THz imaging techniques have been suggested for the investigation of plasmons in 2D materials by combining sub-wavelength spatial resolution with both amplitude- and phase-sensitive detection techniques [6]. Dean *et al.* demonstrated apertureless THz near-field imaging using a quantum cascade laser source, allowing coherent, high-resolution imaging of such structures at room temperature [7], while Mitrofanov *et al.* showed that scanned aperture THz near-field microscopy can reveal surface waves excited at the edges of graphene structures [8]. While the THz response of individual mesoscopic systems can be obtained using such microscopies, accessing the low temperature response <4K is more challenging. Alternative techniques to probe the low temperature broadband (100s of GHz) response of individual mesoscopic systems are therefore required.

Magnetoplasmons are plasmons coupled to a cyclotron resonance driven by magnetic fields. Mast *et al.* reported magnetoplasmons in a classical two-dimensional Coulomb gas of electrons above a liquid-helium surface and observed edge magnetoplasmons (EMPs) for the first time in the frequency range of 0–200 MHz [9]. Since then, EMPs have received significant attention as

#414178 https://doi.org/10.1364/OE.414178
Journal © 2021 Received 4 Nov 2020; revised 3 Mar 2021; accepted 11 Mar 2021; published 13 Apr 2021

Optics EXPRESS

they can be used to study edge-current states in a magnetic field, which are a key factor in the formation of the quantum Hall effect [10,11], as well as being relevant to the recent study of topological insulators [12].

In this paper, we utilise an on-chip THz spectroscopy technique [13,14], which allows the generation and detection of THz current pulses in the plane of a two-dimensional electron gas (2DEG) using an integrated plasmonic circuit [15]. Using this technique, on-chip THz signals are coupled from a coplanar waveguide (CPW) into a 2DEG, by combining the epitaxial of low-temperature-grown gallium arsenide (LT-GaAs) used for THz excitation and detection, with the 2DEG heterostructure [16]. Here, we study the effect of magnetic field on the plasmonic resonances in this system, and also perform full-wave 3D electromagnetic simulations, allowing us to analyze current distributions in the 2DEG and to ascribe the observed excitations unambiguously to bulk and edge magnetoplasmons excited in different regimes of frequency and magnetic field.

2. Results and discussion

Figure 1(a) shows a schematic diagram of the experimental arrangement. The device consists of a 25-μm-wide, 73-μm-long, 120-nm-deep straight mesa etched into the substrate to define the 2DEG channel, onto which an overlaid gate forms three plasmonic coupled cavities (two ungated cavities C_1 (~8.9-μm long), and C_3 (~55-μm long), and one gated cavity C_2 (~9.2-μm long) as shown in Fig. 1(b)). The length of the gated cavity C_2 was chosen to place its fundamental resonance close to 50 GHz, corresponding to the lower end of our accessible bandwidth.

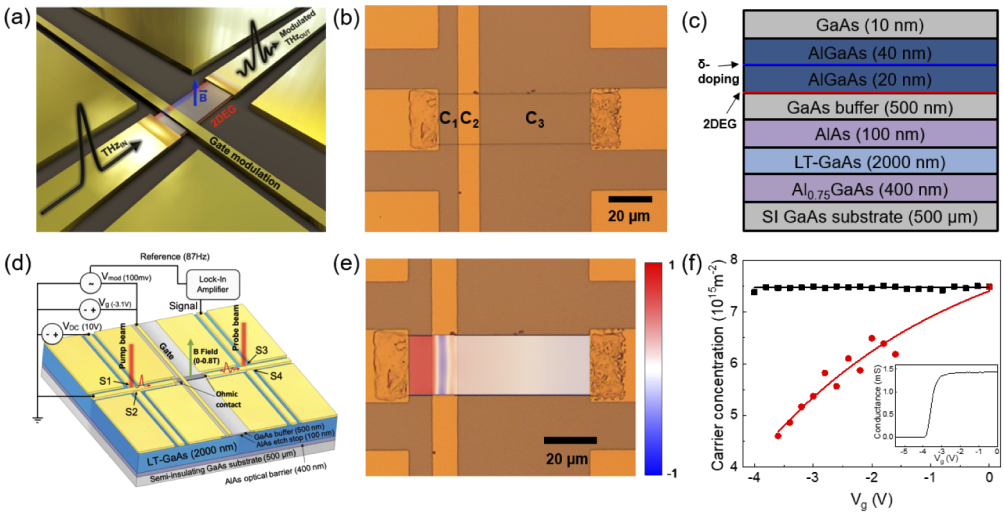


Fig. 1. (a) Schematic of on-chip THz spectroscopy for observation of magnetoplasmons in a 2DEG channel integrated into the CPW. (b) An optical image of the 2DEG channel and CPW. A gate (9.2-μm wide) was fabricated on top of the 2DEG channel, with lengths of the ungated regions on either side of the gate being 8.9 μm and 55 μm. (c) The layer structure of the wafer monolithically integrating the LT-GaAs and GaAs/AlGaAs heterostructure containing the 2DEG layer (red line) (d) A diagram of the THz plasmonic circuit and the electrical connections for the gate-modulation measurement. S1/S2 and S3/S4 are two pairs of PC switches, which are used to generate or detect the THz pulses. (e) Simulated current density along the 2DEG channel at 130 GHz. Red (blue) colour represents the current density pointing to the right (left). (f) The low temperature (T = 2 K) carrier concentrations in the gated (red circles), and ungated (black squares) cavities as a function of the gate bias obtained by two-terminal magnetoresistance measurement. (inset) Two-terminal conductance of 2DEG channel as a function of V_g.

Optics EXPRESS

The layer structure of the wafer, which was prepared by molecular beam epitaxy (MBE), is shown in Fig. 1(c). Figure 1(d) shows the device details and the electrical connections used for measurements. The mesa was first defined in the GaAs/AlGaAs heterostructure containing the 2DEG layer (see Fig. 1(c)) using a sulphuric acid: hydrogen peroxide: water wet etch (H_2SO_4:H_2O_2:H_2O = 1:8:70). Ohmic contacts (200-nm-thick Au-Ge-Ni alloy, annealed at 430°C for 80 secs) were formed at each end of the 2DEG mesa to allow injection of the THz pulses into the 2DEG layer. A CPW was next patterned on the wafer surface, and metallized using electron-beam evaporation of Ti/Au (10/150nm). Pairs of LT-GaAs photoconductive (PC) switches (shown as S1/S2 and S3/S4 in Fig. 1(d)) were defined by the CPW probe arms at either side of the 2DEG mesa to generate or to detect THz pulses upon illumination by an 800 nm wavelength, mode-locked Ti:sapphire laser producing 100-fs-duration pulses at a repetition rate of 80 MHz. Finally, a gate was patterned lithographically and then metalised by electron-beam evaporation and subsequent lift-off, forming a Ti/Au (10/60-nm)-thick strip across the 2DEG mesa that was used both to control the carrier concentration in the 2DEG channel directly underneath the gate, and to modulate the propagating THz pulses. THz pulses were generated by laser pulse excitation of PC switch S1, which was biased at 10 V dc and coupled into the CPW. The signal transmitted through the 2DEG channel was then detected at PC switch S3, which was excited by a time-delayed probe beam split-off from the same laser beam which was incident on S1. To measure the transmitted signal, a gate-modulation technique was used in which an ac voltage of 100 mV RMS at 87Hz was superimposed onto the gate bias allowing lock-in detection to enhance the signal-to-noise ratio [16]. The gate voltage V_g was swept from 0 to −3.6 V dc to investigate the dependence of the plasmon resonance on the carrier concentration. A magnetic field was applied normal to the 2DEG plane and swept from 0 to 0.8 T.

Two approaches were used to model experimental measurements. The first was to estimate the resonant frequencies of the bulk plasmon using the dispersion relation

$$f_p = \sqrt{\frac{n_s e^2}{8\pi^2 m^* \varepsilon_0 \varepsilon_{eff}(k)}}k, \tag{1}$$

where e and m^* are the charge and effective mass of electrons in GaAs, respectively, ε_0 is the vacuum dielectric permittivity, $\varepsilon_{eff}(k)$ is the effective relative permittivity, and k is the plasmon wave number [17], which was assumed to satisfy the multiple-half-wavelength resonance condition. The effective relative permittivity in the gated region is given by $\varepsilon_{eff}(k) = [\varepsilon_2 + \varepsilon_1 \coth(kd)]/2$, where ε_1 and ε_2 are the relative permittivity of AlGaAs ($\varepsilon_1 = 11.5$) and GaAs ($\varepsilon_2 = 12.4$), respectively, and d is the distance from the metallic gate to the 2DEG layer ($d = 75$ nm) [18]. The bulk magnetoplasmon frequencies, f_{mp}, were then found using:

$$f_{mp}{}^2 = f_p{}^2 + f_c{}^2, \tag{2}$$

where $f_c = eB/2\pi m^*$ is the cyclotron frequency [19,20]. This approach is, however, only able to estimate the resonant frequencies of uncoupled cavities. Detailed 3D simulations were therefore performed using a full-wave electromagnetic model [21]. The model included both the 2DEG structure and the CPWs either side. All aspects of the geometry were chosen to be the same as those used in the experiment. The mesa and CPWs rested on a GaAs substrate of a height 30 μm, and had an equal height of air above them. These heights were found to be large enough to permit enclosing the computational domain by conducting boundaries without affecting the plasmon propagation in the 2DEG. The gate, the Ohmic contacts, and the waveguides were also modelled as perfect conductors.

The 2DEG was modelled by a surface current concentration coupled to Maxwell's equations. An additional relationship between the current concentration J and the electric field strength E in

Optics EXPRESS

the x-y plane of the 2DEG was found from the hydrodynamic equations of motion as

$$\begin{pmatrix} J_x \\ J_y \end{pmatrix} = \frac{e^2 n_s}{m[\omega_c^2 + (\gamma + i\omega)^2]} \begin{pmatrix} \gamma + i\omega & \omega_c \\ -\omega_c & \gamma + i\omega \end{pmatrix} \begin{pmatrix} E_x \\ E_y \end{pmatrix} \tag{3}$$

Here ω is the angular frequency, ω_c is the angular cyclotron frequency, and γ is the effective collision frequency. A value of ~140 GHz for the latter was used, which has previously been found to give good agreement with experiments [21]. In the simulations, the field distribution of the CPW eigenmode was first computed at a fixed frequency and then launched at the input of one of the waveguides. The mode reflection coefficient and its transmission coefficient to the waveguide at the opposite end were then calculated, and this then repeated for a range of frequencies and, depending on the experiment modeled, either for a range of gate voltages or for a range of magnetic fields. To model the nonuniform spectrum of the experimental excitation pulse, the simulated spectra were scaled assuming an exponential decay of the excitation power with frequency. The gate-modulation measurements were modelled as numerical approximations of the derivative of the transmission coefficient with respect to voltage. Figure 1(e) shows simulation results on normalised current density of plasmonic mode excited at 130 GHz along the 2DEG channel when the electron concentration in the gated, ungated cavities are 5.2×10^{15} m^{-2}, and 7.5×10^{15} m^{-2}, respectively.

Figure 1(f) shows the carrier concentration in the gated and ungated 2DEG regions for V_g in the range of 0 – −4 V. To obtain these concentrations, the two-terminal resistance of the 2DEG channel was measured as a function of magnetic field at 2K. An ac voltage of 100 μV RMS at 77 Hz was applied across the 2DEG and the center conductor of the CPW, with a dc bias applied to the gate, and a lock-in amplifier was used to measure the differential conductance in a standard constant voltage configuration. The second derivative of resistance with respect to the magnetic field (d^2R/dB^2) shows two oscillations of different periods, corresponding to Shubnikov-de Haas oscillations in the gated and ungated cavities, which we assume to act independently as in our prior experiments [16]. The electron concentrations, n_s, in the gated and the ungated cavities were each obtained using the relationship $\Delta(1/B) = 2e/n_s h$, where e is the elementary charge and h is Planck's constant [22]. The electron concentration in the gated cavity was found to decrease from 7.5×10^{15} m^{-2} to 4.6×10^{15} m^{-2} as the negative gate bias was increased, V_g, from 0 V to −3.6 V, while the n_s in the ungated cavity remained at a constant value of 7.5×10^{15} m^{-2}; we note that in the range of V_g from - 0.2 V to – 1.4 V, the Shubnikov-de Haas oscillations in the gated cavity were indistinguishable from those of the ungated cavity. The inset of Fig. 1(f) shows the two-terminal conductance of the 2DEG channel as a function of the V_g, with the channel pinch-off voltage occurring at a gate bias of ~ −4 V.

Figure 2(a) shows gate-modulation signals obtained at 2K for a center dc voltage of $V_g = -3.1$ V with ac voltage (+/- 100 mV) superimposed, when a THz pulse propagating towards PC switch S3 was generated at PC switch S1 using a dc bias of 10 V. The transmitted signals show clear periodic oscillations that satisfy the Fabry-Pérot resonance conditions as the propagating pulses pass through the 2DEG channel. Figure 2(b) shows a fast Fourier transform (FFT) spectrum of the signal in Fig. 2(a). Four resonances are observed clearly, at 57 ± 17 GHz, 132 ± 17 GHz, 215 ± 17 GHz, and 269 ± 17 GHz. The error of ± 17 GHz was estimated from the FFT frequency resolution, which was determined by the length of the time-domain scan used. The corresponding frequencies of the first four plasmon resonances calculated from Eq. (1) are $f_{1,\mathrm{pred}} = 68$ GHz, $f_{2,\mathrm{pred}} = 135$ GHz, $f_{3,\mathrm{pred}} = 200$ GHz, and $f_{4,\mathrm{pred}} = 263$ GHz.

We then studied the dependence of the plasmon resonances on carrier concentration in the gated cavity by measuring time-domain gate-modulation signals as a function of V_g in Fig. 2(c). The oscillation period is seen to increase as the gate bias is increased negatively, indicating a decrease in plasmon resonant frequencies owing to a reduction in carrier concentration beneath

Optics EXPRESS

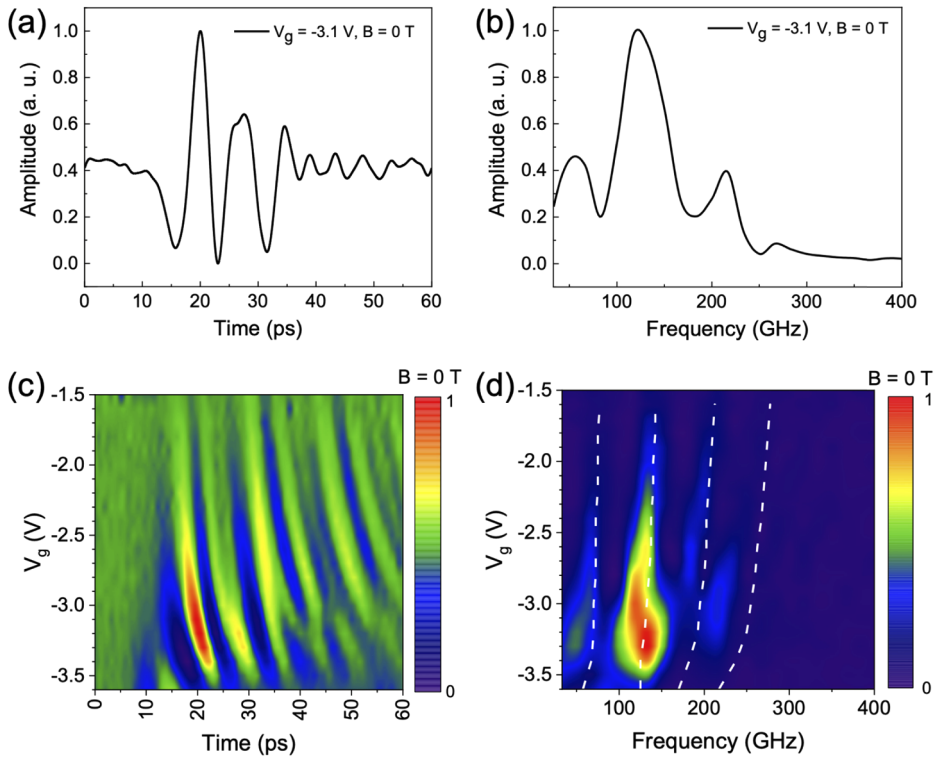


Fig. 2. (a) Gate-modulation signals as a function of time for $V_g = -3.1$ V, in which the THz pulses propagate from S1 to S3 at 2 K (b) The FFT spectrum of the gate-modulation signals measured at $V_g = -3.1$ V. (c) A color-scale plot of the measured gate-modulation signals plotted as a function of time and V_g. (d) A color-scale plot of the FFT amplitude for gate-modulation signals plotted as a function of frequency and V_g, with white dashed lines showing the positions of the first four resonances obtained from full-wave simulations

the gate. The gate modulation signal was strongest at $V_g = -3.1$ V as the carrier concentration in the gated cavity changes dramatically at this bias as shown in Fig. 1(f) [16]. Figure 2(d) shows corresponding FFT spectra of the time-domain measurements. The plasmon resonances showed a red shift as V_g was swept from −1.5 to −3.6 V, while the amplitude of the resonances was strongest at $V_g = -3.1$ V, as expected from the time-domain results. The dashed white lines in Fig. 2(d) show the predicted positions of the first four resonances obtained from full-wave simulations. Agreement with measured positions is excellent for the first three resonances, whereas for the fourth resonance, the agreement is good only for V_g greater than −2.5 V. The deterioration of the agreement between experiment and theory close to the pinch-off voltage may be due to the rapid variation of the electron concentration in this region, leading to a breakdown of the relationship between the gate voltage and the electron concentration modeled from Fig. 1(f). We note that neither the experimental nor the simulated data show evidence of resonances from the ungated 2DEG regions (the lowest of which is predicted to lie around 200 GHz), since the gate-modulation technique employed is anticipated to be relatively insensitive to any resonances which are independent of gate voltage [16].

To investigate the formation of magnetoplasmons in the 2DEG cavity in a magnetic field, we also measured the fine structure of the gate-modulation signals at 2K as a function of magnetic field in the range of 0–0.8 T, with a step of 0.02 T. Figure 3(a) shows gate-modulated time-domain signals measured at $V_g = -3.1$ V for B = 0, 0.3, 0.6T as examples. A V_g of −3.1 V was chosen

Optics EXPRESS

both to maximize the gate-modulation signal, but also to keep the plasmon resonances within our accessible bandwidth. For B = 0, periodic oscillations are observed, consistent with our earlier measurements (Fig. 2(a)); these oscillations change periodicity as magnetic field is applied. To study the evolution of the oscillating signals, Fig. 3(b) shows the gate-modulation signals as a function of magnetic field measured for $V_g = -3.1$ V dc, where signal was the strongest. Figure 3(c) shows FFT spectra of the time-domain measurements shown in Fig. 3(b), while Fig. 3(d) shows the results of full-wave modelling under identical conditions. Both simulation and measurement show two different regions separated by the cyclotron frequency (indicated by dashed orange lines). For any given value of magnetic field, at frequencies higher than the corresponding cyclotron frequency, several distinct features are observed: three in the measured signals (at 52, 128, and 215 GHz at B = 0 T), and five in the simulated response (at 68, 130, 190, 250, and 315 GHz at B = 0 T). The two highest simulated resonances were not observed experimentally owing to a reduction in generated THz-signal intensity at higher frequencies. The white dashed lines show the evolution of the observed above-cyclotron resonances with magnetic field, calculated according to Eq. (2). Both the measured and simulated signals follow the predicted behaviour, although there are variations in the signal strength along individual lines. As shown later, these features correspond to the excitation of bulk magnetoplasmons in the gated cavity.

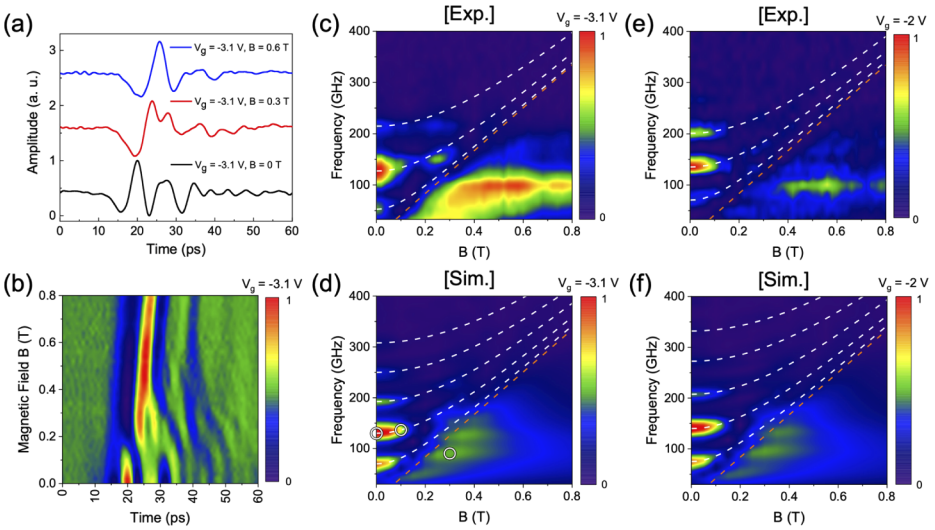


Fig. 3. (a) Time-domain gate-modulation signal measured at $V_g = -3.1$ V and for B = 0, 0.3, and 0.6 T at 2 K. Traces are normalized to the maximum value, and separated from each other with a vertical offset of 1.1. (b) Color-scale plot of the time-domain gate-modulation signals at $V_g = -3.1$ V as a function of magnetic field B. Color-scale plot of the FFT amplitude for gate-modulation signals plotted as a function of frequency and magnetic field for experiment and simulation at $V_g = -3.1$ V (c and d), and for $V_g = -2$ V (e and f). The dashed orange line is the calculated cyclotron resonance frequency and the dashed white lines are the predictions from Eq (2) using resonances at B = 0 T.

Figures 3(e) and 3(f) show additional measured and simulated gate-modulation signals respectively, this time taken at $V_g = -2$ V; these show similar features to those observed in Figs. 3(c) and 3(d). Above the cyclotron frequency, there are several resonances that follow the behaviour predicted by Eq. (2) for bulk magnetoplasmons. At B = 0 T, three measured resonances are observed at 70, 136, and 200 GHz with the corresponding simulated resonances predicted at

Optics EXPRESS

75, 140, and 205 GHz. There is good agreement between the measured and simulated values above the cyclotron line.

In all measurements and simulations across a range of gate biases, a broad feature occurring at ~100 GHz is observed below the cyclotron line. As follows from Eq. (2), bulk magnetoplasmons do not propagate below the cyclotron line. Electron motion corresponding to a bulk plasmon has a longitudinal component and a circular component, the latter being induced by the magnetic field. In the limit of high magnetic field, the circular component dominates, the electron motion is determined by the cyclotron resonance, and $f = f_c$. Electron motion at the edges is, however, restricted, and edge magnetoplasmons may exist that are not bound by the cyclotron resonance. Noting that bulk magnetoplasmons should not therefore propagate below the cyclotron resonance [23], this feature tentatively suggests the presence of edge magnetoplasmons in the 2DEG channel. To further understand the origin of these features, detailed simulations of the current distribution in the 2DEG were performed under three conditions, chosen to correspond to key regions of the data, at B = 0 T and f = 130 GHz, B = 0.1 T and f = 135 GHz, and B = 0.3 T and f = 90 GHz, as indicated by white circles in Fig. 3(d).

Figures 4(a), 4(c), and 4(e) show two-dimensional representations of the normalised current density along the 2DEG as a function of position in the plane of the simulated structure. Figures 4(b), 4(d), and 4(f) show line plots of the same current density simulations, taken along the middle and the top and bottom edges of the 2DEG. The position of the gated region is shown by dashed vertical lines. In the absence of magnetic field, in Figs. 4(a) and 4(b) the current density remains similar for any value of y-position along the width of the 2DEG, with a single peak along the x-axis within the gated region, indicating excitation of a bulk, gated plasmon resonance. At B = 0.1 T and f = 135 GHz, as shown in Figs. 4(c) and 4(d), the bulk gated resonance still dominates everywhere apart from the top edge, where excitation of a higher-order edge plasmon can be seen. However, no significant bulk excitations can be seen below the cyclotron frequency, for example at B = 0.3 T and f = 90 GHz, as shown in Figs. 4(e) and 4(f). The current density here is concentrated along the edges, with the top-edge excitation being dominant. Along this

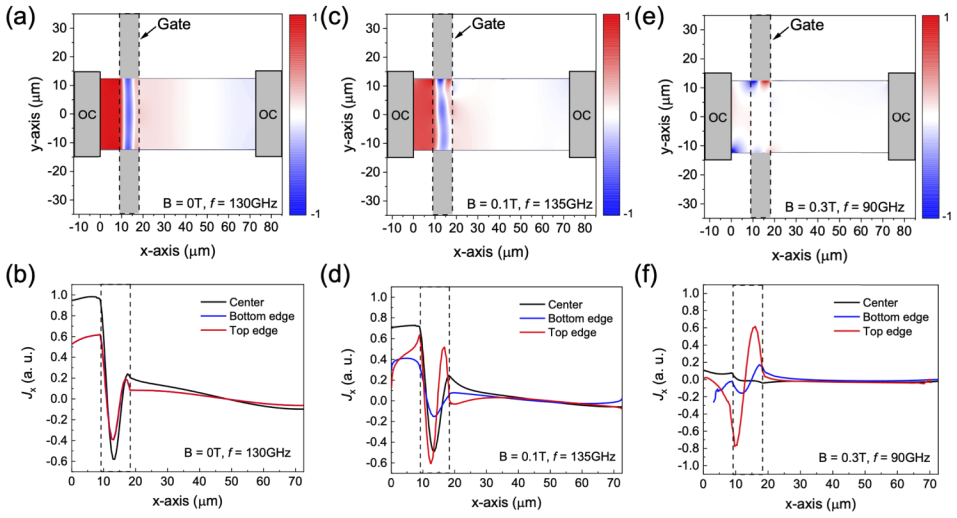


Fig. 4. Simulated current distribution (J_x) in the plane of the 2DEG channel for $V_g = -3.1$ V at (a) B = 0 T, f = 130 GHz, (c) B = 0.1 T, f = 135 GHz, and (e) B = 0.3 T, f = 90 GHz. J_x calculated along the lines across the middle (y = 0), top (y = 12.5 μm), bottom (y = −12.5 μm) of the 2DEG channel at (b) B = 0 T, f = 130 GHz, (d) B = 0.1 T, f = 135 GHz, and (f) B = 0.3 T, f = 90 GHz. Vertical dashed lines represent the gated region. OC: Ohmic contacts

Optics EXPRESS

top edge, a distorted one-wavelength pattern can be seen, comprising an edge plasmon resonance in the gated region. To confirm further that gated edge plasmons are responsible for the signals below the cyclotron frequency, structures were simulated with reduced loss with an effective scattering time increased to 50 ps, and for parametrically varied dimension including the 2DEG width (15–30 μm) and depth (35–75 nm), and the length of the gated region (5–10 μm). We observed that the frequency of the below-cyclotron resonance changed when the length of the gated section and the mesa height were modified, but did not depend appreciably on the 2DEG width. We note that the experimental and simulation techniques used in this work also can be adopted to probe magnetoplasmon modes predicted in other Drude-like two-dimensional materials including topological 2D systems [12], as well as graphene [24].

3. Conclusions

We have observed the evolution of magnetoplasmon resonances in a 2DEG at frequencies up to ~400 GHz and as a function of magnetic field. The observed resonances are reproduced by with 3D full-wave simulations of the system. Analysis of the current distribution in the 2DEG allows us to firmly attribute the resonances above the cyclotron frequency to the excitation of the bulk gated magnetoplasmons, and in the case of those below the cyclotron frequency to the excitation of edge magnetoplasmons in the gated 2DEG region. We anticipate that this work will contribute to the understanding of origin and evolution of the plasmonic effects in 2DEG systems in the THz frequency range, and note that our experimental and theoretical approaches can both be extended to other low-dimensional mesoscopic systems and materials.

Funding. Engineering and Physical Sciences Research Council (EP/P021859/1, EP/R004994/1, EP/R00501X/1); National Natural Science Foundation of China (61701219).

Acknowledgments. The authors gratefully acknowledge funding from the EPSRC and from the UK National Physical Laboratory; EHL acknowledges support from the Royal Society and Wolfson Foundation. JBW acknowledges support from the NSFC. The data associated with this paper is available from University of Leeds at https://doi.org/10.5518/818

Disclosures. The authors declare no conflicts of interest.

References

1. B. Sensale-Rodriguez, R. Yan, M. M. Kelly, T. Fang, K. Tahy, W. S. Hwang, D. Jena, L. Liu, and H. G. Xing, "Broadband graphene terahertz modulators enabled by intraband transitions," Nat. Commun. **3**(1), 780 (2012).
2. Y. Zhang, Y. Zhao, S. Liang, B. Zhang, L. Wang, T. Zhou, W. Kou, F. Lan, H. Zeng, J. Han, Z. Feng, Q. Chen, P. Mazumder, and Z. Yang, "Large phase modulation of THz wave via an enhanced resonant active HEMT metasurface," Nanophotonics **8**(1), 153–170 (2018).
3. T. Otsuji, Y. M. Meziani, T. Nishimura, T. Suemitsu, W. Knap, E. Sano, T. Asano, and V. V. Popov, "Emission of terahertz radiation from dual grating gate plasmon-resonant emitters fabricated with InGaP/InGaAs/GaAs material systems," J. Phys.: Condens. Matter **20**(38), 384206 (2008).
4. M. Ali Khorrami, S. El-Ghazaly, S. Q. Yu, and H. Naseem, "Terahertz plasmon amplification using two-dimensional electron-gas layers," J. Appl. Phys. **111**(9), 094501 (2012).
5. F. Teppe, D. Veksler, V. Y. Kachorovski, A. P. Dmitriev, X. Xie, X. C. Zhang, S. Rumyantsev, W. Knap, and M. S. Shur, "Plasma wave resonant detection of femtosecond pulsed terahertz radiation by a nanometer field-effect transistor," Appl. Phys. Lett. **87**(2), 022102 (2005).
6. M. C. Giordano, L. Viti, O. Mitrofanov, G. Scamarcio, S. Mastel, R. Hillenbrand, D. Ercolani, L. Sorba, and M. S. Vitiello, "Sub-wavelength near field imaging techniques at terahertz frequencies," in *Proc. SPIE Int. Soc. Opt. Eng.* 105400N (2018).
7. P. Dean, O. Mitrofanov, J. Keeley, I. Kundu, L. Li, E. H. Linfield, and A. Giles Davies, "Apertureless near-field terahertz imaging using the self-mixing effect in a quantum cascade laser," Appl. Phys. Lett. **108**(9), 091113 (2016).
8. O. Mitrofanov, W. Yu, R. J. Thompson, Y. Jiang, I. Brener, W. Pan, C. Berger, W. A. De Heer, and Z. Jiang, "Probing terahertz surface plasmon waves in graphene structures," Appl. Phys. Lett. **103**(11), 111105 (2013).
9. D. B. Mast, A. J. Dahm, and A. L. Fetter, "Observation of bulk and edge magnetoplasmons in a two-dimensional electron fluid," Phys. Rev. Lett. **54**(15), 1706–1709 (1985).
10. Y. P. Monarkha, F. M. Peeters, and S. S. Sokolov, "Edge excitations of a two-dimensional electron solid in a magnetic field," J. Phys.: Condens. Matter **9**(7), 1537–1545 (1997).
11. M. Wassermeier, J. Oshinowo, J. P. Kotthaus, A. H. MacDonald, C. T. Foxon, and J. J. Harris, "Edge magnetoplasmons in the fractional-quantum-Hall-effect regime," Phys. Rev. B **41**(14), 10287–10290 (1990).

Optics EXPRESS

12. D. Jin, L. Lu, Z. Wang, C. Fang, J. D. Joannopoulos, M. Soljačić, L. Fu, and N. X. Fang, "Topological magnetoplasmon," Nat. Commun. **7**(1), 13486 (2016).
13. C. Russell, M. Swithenbank, C. D. Wood, A. D. Burnett, L. Li, E. H. Linfield, A. G. Davies, and J. E. Cunningham, "Integrated On-Chip THz Sensors for Fluidic Systems Fabricated Using Flexible Polyimide Films," IEEE Trans. THz Sci. Technol. **6**(4), 619–624 (2016).
14. N. Hunter, A. S. Mayorov, C. D. Wood, C. Russell, L. Li, E. H. Linfield, A. G. Davies, and J. E. Cunningham, "On-chip picosecond pulse detection and generation using graphene photoconductive switches," Nano Lett. **15**(3), 1591–1596 (2015).
15. C. D. Wood, D. Mistry, L. H. Li, J. E. Cunningham, E. H. Linfield, and A. G. Davies, "On-chip terahertz spectroscopic techniques for measuring mesoscopic quantum systems," Rev. Sci. Instrum. **84**(8), 085101 (2013).
16. J. Wu, A. S. Mayorov, C. D. Wood, D. Mistry, L. Li, W. Muchenje, M. C. Rosamond, L. Chen, E. H. Linfield, A. G. Davies, and J. E. Cunningham, "Excitation, detection, and electrostatic manipulation of terahertz-frequency range plasmons in a two-dimensional electron system," Sci. Rep. **5**(1), 15420 (2015).
17. F. Stern, "Polarizability of a two-dimensional electron gas," Phys. Rev. Lett. **18**(14), 546–548 (1967).
18. M. Shur, "Plasma wave terahertz electronics," Electron. Lett. **46**(26), S18–S21 (2010).
19. V. M. Muravev, I. V. Andreev, I. V. Kukushkin, S. Schmult, and W. Dietsche, "Observation of hybrid plasmon-photon modes in microwave transmission of coplanar microresonators," Phys. Rev. B **83**(7), 075309 (2011).
20. Q. Zhang, T. Arikawa, E. Kato, J. L. Reno, W. Pan, J. D. Watson, M. J. Manfra, M. A. Zudov, M. Tokman, M. Erukhimova, A. Belyanin, and J. Kono, "Superradiant decay of cyclotron resonance of two-dimensional electron gases," Phys. Rev. Lett. **113**(4), 047601 (2014).
21. A. Dawood, J. B. Wu, C. D. Wood, L. H. Li, E. H. Linfield, A. G. Davies, J. E. Cunningham, and O. Sydoruk, "Full-wave modelling of terahertz frequency plasmons in two-dimensional electron systems," J. Phys. D: Appl. Phys. **52**(21), 215101 (2019).
22. C. S. Chang, H. R. Fetterman, and C. R. Viswanathan, "The characterization of high electron mobility transistors using Shubnikov-de Haas oscillations and geometrical magnetoresistance measurements," J. Appl. Phys. **66**(2), 928–936 (1989).
23. G. Ernst, R. J. Haug, J. Kuhl, K. Von Klitzing, and K. Eberl, "Acoustic edge modes of the degenerate two-dimensional electron gas studied by time-resolved magnetotransport measurements," Phys. Rev. Lett. **77**(20), 4245–4248 (1996).
24. A. A. Sokolik and Y. E. Lozovik, "Edge magnetoplasmons in graphene: Effects of gate screening and dissipation," Phys. Rev. B **100**(12), 125409 (2019).

155.198.10.231 {ts '2021-04-20 04:42:04'}